

# **SANDIA REPORT**

SAND2001-8262  
Unlimited Release  
Printed June 2001

## **DETECTION OF SURFACE CONTAMINANT RESIDUE BY TURNABLE INFRARED LASER IMAGING**

David Otteson, Howard Johnsen, Sarah Allendorf, Tom Kulp, Karla Armstrong,  
Scott Robinson, Peter Ludowise, and Uta Goehrs

Prepared by  
Sandia National Laboratories  
Albuquerque, New Mexico 87185 and Livermore, California 94550

Sandia is a multiprogram laboratory operated by Sandia Corporation, a  
Lockheed Martin Company, for the United States Department of Energy  
under Contract DE-AC04-94AL85000.

Approved for public release; further dissemination unlimited.



**Sandia National Laboratories**

Issued by Sandia National Laboratories, operated for the United States Department of Energy by Sandia Corporation.

**NOTICE:** This report was prepared as an account of work sponsored by an agency of the United States Government. Neither the United States Government, nor any agency thereof, nor any of their employees, nor any of their contractors, subcontractors, or their employees, make any warranty, express or implied, or assume any legal liability or responsibility for the accuracy, completeness, or usefulness of any information, apparatus, product, or process disclosed, or represent that its use would not infringe privately owned rights. Reference herein to any specific commercial product, process, or service by trade name, trademark, manufacturer, or otherwise, does not necessarily constitute or imply its endorsement, recommendation, or favoring by the United States Government, any agency thereof, or any of their contractors or subcontractors. The views and opinions expressed herein do not necessarily state or reflect those of the United States Government, any agency thereof, or any of their contractors.

Printed in the United States of America. This report has been reproduced directly from the best available copy.

Available to DOE and DOE contractors from  
U.S. Department of Energy  
Office of Scientific and Technical Information  
P.O. Box 62  
Oak Ridge, TN 37831

Telephone: (865)576-8401  
Facsimile: (865)576-5728  
E-Mail: [reports@adonis.osti.gov](mailto:reports@adonis.osti.gov)  
Online ordering: <http://www.doe.gov/bridge>

Available to the public from  
U.S. Department of Commerce  
National Technical Information Service  
5285 Port Royal Rd  
Springfield, VA 22161

Telephone: (800)553-6847  
Facsimile: (703)605-6900  
E-Mail: [orders@ntis.fedworld.gov](mailto:orders@ntis.fedworld.gov)  
Online order: <http://www.ntis.gov/ordering.htm>



SAND2001-8262  
Unlimited Release  
Printed June 2001

## **DETECTION OF SURFACE CONTAMINANT RESIDUE BY TUNABLE INFRARED LASER IMAGING**

David Ottesen and Howard Johnsen  
Analytical Materials Science

Sarah Allendorf  
Combustion Research Department

Tom Kulp and Karla Armstrong  
Diagnostics & Remote Sensing  
Sandia National Laboratories/CA

Scott Robinson  
Intel Corp., Chandler, AZ

Peter Ludowise  
3M Corp., Maplewood, MN

Uta Goehrs  
Corning, Inc., Corning, NY

### **ABSTRACT**

We report the development of a new, real-time non-contacting monitor for cleaning verification based on tunable infrared-laser methods. New analytical capabilities are required to maximize the efficiency of cleaning operations at a variety of federal (Department of Defense [DoD] and Department of Energy [DOE]) and industrial facilities. These methods will lead to a reduction in the generation of waste streams while improving the quality of subsequent processes and the long-term reliability of manufactured, repaired or refurbished parts.

We have demonstrated the feasibility of tunable infrared-laser imaging for the detection of contaminant residues common to DoD and DOE components. The approach relies on the technique of infrared reflection spectroscopy for the detection of residues.

An optical interface for the laser-imaging method was constructed, and a series of test surfaces was prepared with known amounts of contaminants. Independent calibration of the laser reflectance images was performed with Fourier transform infrared (FTIR) spectroscopy. The performance of both optical techniques was evaluated as a function of several variables, including the amount of contaminant, surface roughness of the panel, and the presence of possible interfering species (such as water). Finally, detection limits for generic hydrocarbon contaminants were evaluated as a function of system noise level.

## **ACKNOWLEDGMENTS**

We gratefully acknowledge the financial support for these investigations by the Department of Defense through the Strategic Environmental Research and Development Program. We also wish to thank Theresa Hoffard, Calvin Kodres, and Daniel Polly of the Naval Facilities Engineering Service Center, Port Hueneme, CA, for the preparation of calibrated samples and FTIR reflectance data.

## Table of Contents

	<b>Page</b>
Title Page .....	3
Acknowledgments .....	4
I. Introduction.....	6
II. Experimental .....	8
Quasi-Phasematching Infrared.....	9
Calibrated Test Sample Preparation .....	14
III. Results and Discussion .....	16
FTIR Measurements .....	17
Turnable Infrared-Laser Imaging .....	26
IV. Conclusions.....	32
V. References.....	34
VI. Distribution .....	35

# **DETECTION OF SURFACE CONTAMINANT RESIDUE BY TUNABLE INFRARED LASER IMAGING**

## **I. Introduction**

We are developing an optical inspection method to help reduce the production of waste streams during cleaning operations. Real-time techniques to provide both qualitative and quantitative assessments of surface cleanliness are needed for a wide variety of governmental and industrial applications. The availability of a convenient analysis technology for on-site, post-cleaning determination of surface contamination will allow more rapid and accurate assessments of the efficiency of chosen cleaning techniques. Overall, this capability will lead to the reduction of hazardous materials usage, handling and disposal, and to improved alternative cleaning products and processes.

The range of government and industrial sites for such a technology is very large with applications such as aircraft, shipboard, vehicle and weapon component surfaces to be coated, plated or bonded. By developing an on-line technique, processed parts or extracted samples will not have to be sent to a separate laboratory for analysis, thereby eliminating processing delays. The information provided by the optical method will assist the process operator in distinguishing between specific contaminants and determining subsequent actions to be taken.

In this paper we report the development of an infrared laser-based imaging approach that will reduce the use, emission and handling of hazardous materials in cleaning operations. This work is supported by the separate development of a hardened, portable Fourier transform infrared (FTIR) reflectance instrument at the Naval Facilities Engineering Service Center (NFESC), Port Hueneme, CA in cooperation with the Surface Optics Corporation. This work is complementary in nature to the laser-imaging technique, and is described in detail elsewhere [Hoffard, et al. 2000]. Both instruments will be used primarily for the real-time on-line or near-line detection of

contaminant residues on reflective surfaces. In each case, surface contamination is detected by its absorption of a grazing-incidence infrared beam reflected from the surface.

The instruments differ in the nature of the information they provide. The laser-based instrument produces images that directly indicate the spatial extent and location of infrared-absorbing surface hydrocarbon contaminants. The FTIR instrument provides a wide-band spectral measurement of the surface reflectance averaged over a small area for nearly all organic materials, and many inorganic components. Thus, the laser-imaging system allows the rapid determination of surface cleanliness for organic residues over a large area, while the spectrally-resolved FTIR method is useful in identifying the specific molecular composition of a surface contaminant at a particular location.

The imaging system being developed employs a widely tunable infrared-laser illumination source in conjunction with an infrared camera. This approach provides an on-line technique for surveying contamination levels over large surface areas in a real-time imaging mode. The laser is broadly-tunable over the 1.3-4.5  $\mu\text{m}$  wavelength range, thus allowing the detection of many hydrocarbon contaminants via absorption bands associated with CH-, OH-, and NH-stretching vibrations.

Currently, the detection and identification of surface contaminants on reflective surfaces is conveniently and rapidly done by FTIR reflectance methods. These non-destructive, non-contacting optical techniques identify the chemical constituents of the contaminants, and can yield quantitative measurements with appropriate calibration. Infrared optical methods are particularly useful for cleanliness analysis since the surface is probed under ambient conditions. More sensitive high-vacuum electron and ion spectroscopic techniques (X-ray photoelectron spectroscopy, Auger electron spectroscopy, and secondary-ion mass spectrometry) are not suited for on-line application.

Commercial instruments that employ infrared reflectance spectroscopy are available for surface analysis and provide both quantitative and qualitative information on surface coatings. These instruments are limited in their ultimate sensitivity to surface contaminants by the nature of their

optical design. Infrared radiation is focused onto the surface to be analyzed at a near-normal angle of incidence, resulting in a compact hand-held apparatus. The infrared light is collected as either specularly or diffusely reflected radiation according to the roughness and scattering properties of the surface [Kodres, et al., 1998a, 1998b]. The resulting sensitivity to very thin layers of surface species is limited by poor coupling of the incident electromagnetic field with the vibrating dipoles of the surface molecular species [Greenler, 1966; Allara, 1977; Golden, 1985] in layers less than 0.1  $\mu\text{m}$  thick.

In order to maximize the sensitivity of infrared reflectance measurements for absorption bands of thin layers of contaminants on metallic surfaces, theoretical and experimental studies [Ottesen, 1985, 1986; Bradshaw, 1987] have shown that the angle of incidence of infrared radiation on the surface should be increased to at least  $60^\circ$  from the surface normal. This is also true for many thin-film residues on the surface of non-metals, such as dielectrics and semiconductors (although the detectability of contaminant absorption bands under these circumstances depends strongly on the optical constants of both surface and substrate, and any absorption features intrinsic to the non-metallic substrate). Additional sensitivity in the reflectance measurement is obtained by measuring only the component of the reflected infrared radiation polarized parallel to the plane of incidence. This experimental method is variously referred to as, “grazing-angle” reflectance spectroscopy or infrared reflection-absorption spectroscopy (IRRAS), and underlies the sampling method of our newly developed tunable-laser imaging device.

## **II. Experimental**

The laser-based instrument described in this report offers the capability to rapidly survey large surface areas and to determine the location and extent of residual hydrocarbon contaminants following cleaning operations. In contrast, an FTIR-based infrared reflectance analysis is able to characterize a very broad range of organic constituents and many inorganic species. However, a surface-probing FTIR instrument measures a spectrum at only a single small area on a sample, thus requiring broad area surveys to be done by sequentially probing many points. Even at a rate of  $\sim 10$  seconds per measurement point, this can be a time-consuming process. The rate of measurement by FTIR spectroscopy is constrained by the

relatively low spectral brightness (compared to a laser) of the incandescent illumination sources. This makes it necessary to use relatively long integration times to achieve an acceptable signal-to-noise ratio.

The tunable-laser-based instrument overcomes these limitations by illuminating a broad surface area with a high-brightness infrared laser. This approach allows a single-wavelength reflectance measurement over an area of several square centimeters to be made on a timescale of a second. Measurements at multiple wavelengths are conducted by tuning the laser and acquiring the image at each desired wavelength. While a detailed spectral map of a surface can be generated over the laser tuning range, the primary use of the system is to provide rapid areal surveys at a few key wavelengths that are indicative of hydrocarbon contaminants. The detection sensitivity for several hydrocarbon species at various illumination wavelengths was evaluated in this work, as well as a method to suppress image noise due to laser speckle while maintaining high illumination intensity.

### **Quasi-Phasematching Tunable Infrared Laser**

The broadly-tunable infrared laser illuminator is based on a technology called quasi-phasematching (QPM) [Powers, et al., 1997]. This approach has been exploited to increase the tuning range and power of the infrared light source while reducing its size. For example, continuous-wave optical parametric oscillators (OPOs) that employ the QPM material, periodically-poled lithium niobate (PPLN), are capable of tuning over the full 1.3-4.5  $\mu\text{m}$  spectral region while emitting more than 0.5 W of power. This technique has been used to generate tunable infrared laser light for imaging natural gas emissions, and developing laser-based spectroscopic gas sensors. In this work we are extending it to the analysis of hydrocarbon residues on material surfaces.

The current tuning range of the PPLN-based laser is limited at long wavelengths to about 4.5  $\mu\text{m}$  due to the transmission characteristics of lithium niobate. This property restricts the sensitivity of the chemical imaging system to functional groups containing hydrogen atoms (C-H, N-H, O-

H). Extension of the laser tuning range beyond 5- $\mu\text{m}$  wavelength is desirable to afford specific identification of hydrocarbon and some inorganic molecular species.

The light source assembled for the IR imaging sensor is an OPO pumped by a continuous-wave (cw) Nd:YAG laser, as shown in Figure 1 [Powers, et al., 1997]. An electric field is induced in the OPO's PPLN crystal by the electric field of the pump laser; these fields interact to form two new laser beams whose frequencies sum to the frequency of the pump laser. The reflectivities of the mirrors in the optical cavity are selected to resonate one of the generated waves, while the other wave is simply generated and released from the cavity. The resonated wave is called the signal; the nonresonated wave is called the idler. The exact frequencies of the signal and the idler are determined by the phasematching properties of the crystal (described below), the reflectivity of the cavity, and by any spectrally-selective optics that may be placed in the cavity. While either the signal or the idler beam can be used for measurements, only the idler is used in the experiments reported here.

As shown in Figure 1, the OPO used in the imaging sensor is of the "bowtie-ring" design. A diode-pumped, cw, multimode Nd:YAG laser (Lightwave Electronics) that is capable of generating at least 6 W of output power at 1064 nm is used as the OPO pump source. Two flat mirrors (M3 and M4) and two curved mirrors (M1 and M2, 50-mm radius of curvature), all coated to be highly reflective at the signal and highly transmissive at the pump and idler wavelengths, form the bow-tie-shaped singly resonant ring oscillator designed to resonate the signal wave. An anti-reflection-coated lens, positioned between the pump laser and the OPO cavity, serves to image the gaussian pump beam into the PPLN crystal. In this way, a beam waist (E-field radius) of 70  $\mu\text{m}$  is created in the center of the crystal, which itself is centered between the two curved cavity mirrors. During normal operation, the OPO resonates on a single signal mode for minutes at a time, whereupon it hops to another cavity mode. The idler bandwidth is, however, determined by that of the pump beam, which is 10–15 GHz.

The use of the QPM material, PPLN, makes cw OPO operation more tunable and efficient than it would be for a conventional birefringently phasematched crystal. Simply stated, phasematching is a condition in which all of the interacting waves (i.e., signal, pump, idler) maintain a specified

relative phase relationship as they propagate through a nonlinear medium, and is a necessary condition for efficient nonlinear generation. In birefringent materials, phasematching is achieved by careful selection and/or control of the crystal birefringence, temperature, and beam propagation angles.

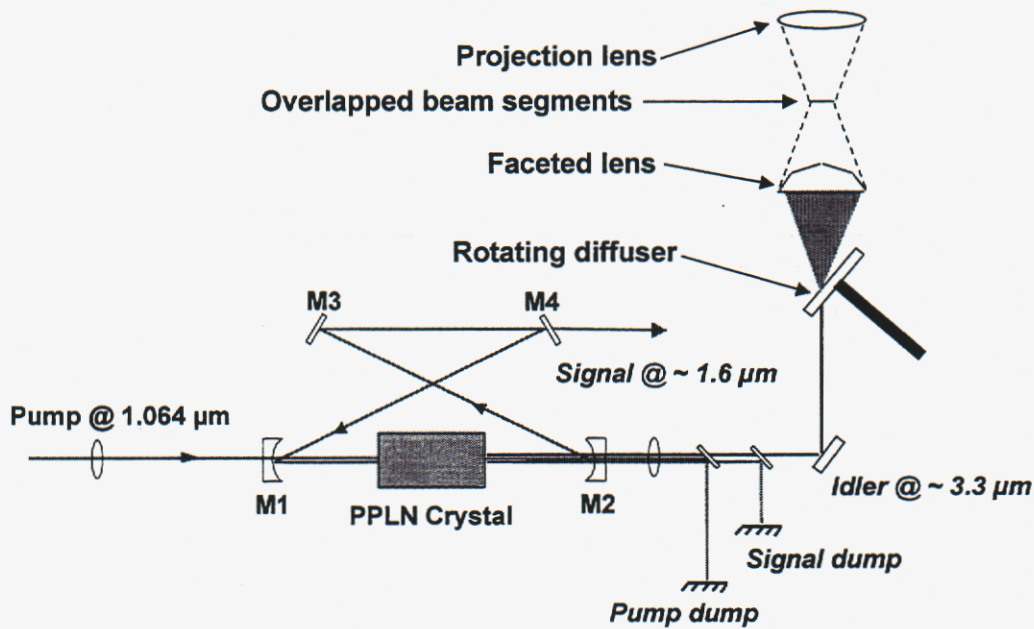


FIGURE 1. Diagram of the PPLN OPO and projection optics.

In a QPM medium, phasematching is engineered into the medium by causing the crystal to have a periodically inverting optical axis (see Figure 2). The engineering process increases conversion efficiency by allowing the use of much stronger nonlinear coefficients of the crystal, and frees the system from reliance on birefringence thereby increasing tunability. As the light beams cross the crystal-axis-inverting boundaries, any relative dephasing of the waves is corrected. For a crystal of a given periodicity, the rephasing is effective for a particular set of pump, signal, and idler frequencies. Some degree of tuning of these waves can be achieved within the crystal phasematching bandwidth (typically  $10\text{-}20 \text{ cm}^{-1}$ ). Broader tuning is achieved

by accessing a portion of the same crystal having a different periodicity, or by changing the temperature of the crystal. The “fanout” grating configuration in Figure 2, for example, allows the periodicity to be continuously changed by translating the crystal through the pump laser beam.

In the present system, two 50-mm-long PPLN crystals (Crystal Technology) with an aperture of 11.5 mm × 0.5 mm are used as the active medium. Each contains eight poled regions having different periodicities ranging from 28.5 to 29.9  $\mu\text{m}$ , and from 30.0 to 31.2  $\mu\text{m}$ . When operating at a crystal temperature of 148°C, these periods collectively allow tuning of the idler from 2720 to 3702  $\text{cm}^{-1}$ . The crystals are mounted in a stacked fashion within a temperature-stabilized copper oven that is attached to a vertical translation stage. Each crystal is tuned by selecting a period using the vertical motion of the stage; horizontal motion of the oven is used to select one crystal or the other.

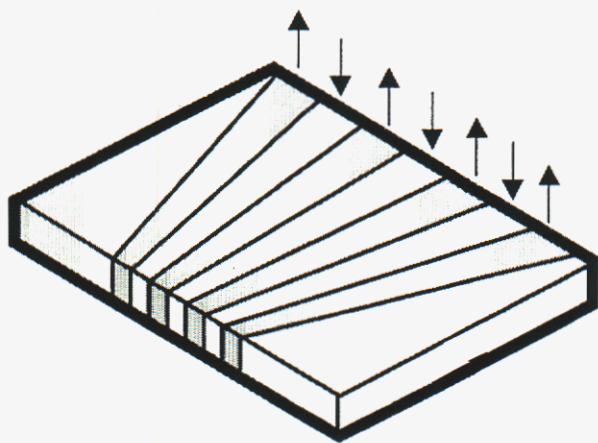


FIGURE 2. Schematic diagram of a “fan-out” PPLN crystal, in which the period continuously varies across the crystal width. The arrows indicate the orientation of the crystallographic z-axis. In reality, the periods of inversion are much narrower than indicated (typically  $\sim 28\text{-}31 \mu\text{m}$ ).

The raw output of the OPO contains the idler beam as well as portions of the signal and pump beams and some higher-order (red, green) beams created spuriously in the PPLN crystal. Spectral filtering is used to dump all but the idler beam. Prior to illumination of the sample, the idler is passed through a set of projection optics, also shown in Figure 1. The first of these is a

ZnSe diffuser (mean roughness of  $\sim 3\text{-}4\ \mu\text{m}$ ) that is mounted on a motor-driven spindle. The diffuser serves to reduce the phase coherence of the idler in order to minimize laser speckle noise in the transmitted beam and the reflected light viewed by the IR camera. The cone of radiation leaving the diffuser is collected by a ZnSe faceted lens (Laser Power Optics). The faceted lens is formed to contain the equivalent of 16 1/4" facets and 16 partial facets around the edge of the lens on a 1.5" diameter with an effective f-number of 1.7. It operates as a prism array – the expanded beam is segmented into 32 different square beamlets that are subsequently overlapped at a distance of 2" from the surface of the lens. The square-shaped overlap region is then imaged onto the target using an f/1.7, 3.3" focal-length ZnSe lens. As a unit, the system converts the gaussian profile of the idler beam into a uniform square illumination on the sample surface.

The infrared laser light is incident on the sample surface at an angle of  $60^\circ$  from the surface normal, and the specularly reflected component is detected by an InSb focal-plane array (FPA) camera with an infrared macro-lens assembly and an array size of  $256 \times 256$  pixels. The FPA camera is located approximately 0.3 m from the sample surface, and the resulting field of view is  $20 \times 35$  mm. Future work will enlarge both the laser illumination area and image field of view in order to develop a prototype instrument capable of rapid large-area surveys during cleaning verification.

FTIR instrumentation at both Sandia and NFESC was used to characterize the mid-infrared spectra of contaminated surfaces via optical interfaces for grazing-angle reflectance spectroscopy. The system at NFESC uses a commercially available sampling accessory that permits a variable angle of incidence from  $30$  to  $80^\circ$ , which is convenient for evaluating detection limits for contaminants on a variety of surfaces. The optical interface at Sandia was constructed with a fixed  $60^\circ$  angle of incidence with optics external to the spectrometer. It also differs from the NFESC system in the large solid-angle used both to illuminate the surface and collect reflected light. This feature is particularly useful in the examination of rougher surfaces that cause significant scattering of the infrared beam, with a consequent degradation in both signal/noise ratio and detection limits. Both systems use infrared polarizers to enhance the sensitivity of the measurements by restricting the surface illumination to p-polarization

[Greenler, 1966]. Unless otherwise noted, all reflectance spectra presented in this report are for p-polarized measurements.

### **Calibrated Test Sample Preparation**

In order to evaluate the usefulness of the laser-imaging technique as a cleaning verification method, we prepared a number of test surfaces with well-characterized levels of contamination. These were used to determine detection limits as a function of contaminant species, level of contamination, degree of surface roughness, effect of spectral interference, and instrumental parameters such as angle-of-incidence. Seven candidate materials were chosen as contaminant species for evaluation as shown in Table 1. These materials have proven to be particularly difficult to remove during cleaning operations, and are representative of many other organic contaminants encountered in government and industrial cleaning processes. Detailed measurements on the first four materials have been made in the course of this work, preliminary measurements have been made on the remaining three.

A number of metals were chosen as substrates for the target contaminants, based on usage information obtained from military and contractor facilities. These were Aluminum-7075-T6, Titanium 6Al-4V, Steel Alloy 4340, Stainless Steel 304, and Magnesium AZ31B. The metals were fabricated into 1.5 x 5 inch flat coupons for laboratory testing and method demonstration.

TABLE 1

## Materials for Calibrated Test Coupon Preparation

<u>Material</u>	<u>Description</u>	<u>Usage</u>
Drawing Agent	White soft solid – ester grease	Metal drawing, cutting, and lubricating agent
Lubricant	Brown liquid – paraffin hydrocarbons	Rust preventative, cleaner, lubricant, protectant for metals
Silicone	Silicone	Lubricant
Mold Release 1	Green liquid – ethenol homopolymer	Mold release agent
Mold Release 2	Clear liquid – proprietary polymeric resins	Mold release agent
Solder Flux	Yellow liquid – abietic acids or anhydrides	Soldering flux for electrical and electronic applications
Hydraulic Oil MIL-H-5606A AM2	Blue liquid – castor oil base	Hydraulic systems, shock & strut lubricant

Six surface roughness finishes of the Aluminum 7075-T6 test coupons were obtained, ranging from 80 to 600 grit (600 grit being the smoothest). A profilometer instrument was used to examine the surface roughness profiles and provide average  $R_a$  values. Due to the nature of metal-shop finishing processes, surface roughness values vary considerably across a given surface area, particularly in orientations longitudinal and transverse to the polishing axis. Finishing operations resulted in a directional “grain” parallel to the sample coupons’ longitudinal direction. Two surface roughness levels, 600 and 220 grit, were obtained for the other metal alloys.

Prior to contaminant application, the aluminum alloy coupons were cleaned with acetone and underwent sonication with a clean-rinsing aqueous cleaner. They were thoroughly rinsed in distilled water and dried in an oven at 50°C. Once cooled, they were weighed on a microbalance with a precision of 0.01 mg. Two or three weighings were averaged.

Both drawing agent and lubricant contaminated Al-7075 coupons were produced by two primary deposition methods – airbrushing and manual brushing. Several other techniques were attempted, including “wire-cator” drawing, coupon spinning, and “manual drop and spread.” These techniques were not used to produce calibrated test samples for these particular contaminants due to the superior results obtained from airbrushing and manual brushing. Three levels of drawing agent were applied by airbrushing to three Al test coupons for each of six surface finishes, creating a suite of 18 panels. Varying concentrations of drawing agent in water were prepared for the airbrush solutions. Similarly, four levels of lubricant were applied to four Al test coupons for each of six surface finishes, creating a suite of 24 panels. Manual brushing was used for all but the least contaminated samples, which were airbrushed. Lubricant solutions for both techniques were prepared using a pentane solvent matrix. Similar methods were used in preparing calibrated samples of the mold release, solder flux, and hydraulic oil samples.

All contaminated coupons were gently heated in an oven at 50°C for several days to remove semi-volatile and volatile components. This served to stabilize the contaminants, allowing for quantification by weighing. Once the weights became stable, the coupons were cooled and weighed to determine the amount of contaminant present on the surface. When not being weighed or scanned, the coupons were kept in a desiccator.

### **III. Results and Discussion**

Grazing-angle incidence reflectance spectroscopy acts to enhance detection sensitivity for thin layers of residue predominantly through improved coupling of the electric field intensity of the incident beam with the vibrating dipoles of the surface contaminant layer perpendicular to the metallic surface. Some additional enhancement of the infrared absorption spectrum will also occur due to a lengthening of the effective path length through the absorbing thin film layer. The general approach is outlined in Figure 3 for an infrared beam incident on a contaminant-laden surface with average film thickness,  $d$ .

If the optical properties of both thin film and substrate are known (or can be determined), the reflection-absorption spectrum can be calculated as a function of film thickness and angle of

incidence. This capability is particularly useful for interpreting experimental data and designing optical instrumentation. Computer codes written at Sandia [Ottesen, 1985] performed these calculations for a variety of materials.

### **FTIR Measurements**

FTIR reflectance data for the full drawing-agent sample set were obtained at NFESC and Sandia using angles of incidence of 75 and 60° for average film thickness ranging from 0.1 to 1  $\mu\text{m}$ , and aluminum substrates with surface finish ranging from 600 to 80 grit. Since the surface finishing operation produced a highly directional roughness, measurements were made both longitudinally and transversely with respect to the polishing grooves.  $R_a$  values were determined at NFESC using profilometer measurements, and resulted in surface roughness values of 0.3 to 1.5  $\mu\text{m}$  for the longitudinal direction, and 0.5 to 6  $\mu\text{m}$  for the transverse direction.

The FTIR reflectance spectra were normalized using the uncoated back of a panel as a clean reference standard, and the intensity data are presented as either reflectance or  $-\log$  reflectance in the following discussion. The C-H stretching vibrations near 2900  $\text{cm}^{-1}$  proved to be generally useful in quantifying instrument response since these frequencies are well isolated from atmospheric interference due to water vapor and carbon dioxide. However, the baseline for these reflectance data was often non-linear. A simple single-point measurement of intensity was therefore not sufficient to determine the instrument response function.

Optical constants ( $n$  and  $k$ ) were derived for the contaminant C-H stretching vibrations using the Sandia reflectance code and a dispersion model to calculate a fit to the experimental data for one of the test coupons [Ottesen, 1985]. Reflectance-absorption spectra for the 2800 – 3000  $\text{cm}^{-1}$  range were calculated for 1- $\mu\text{m}$  thick films of a specific hydrocarbon contaminant on an aluminum surface at either 60 or 75° angle of incidence. This function was then used as a linear variable in conjunction with a second-order polynomial to produce a least-squares fit of the experimental reflectance data for the test coupons. An example is shown in Figure 4 for the longitudinal measurements of three thicknesses of drawing-agent contaminant at 75° angle-of-incidence. This procedure produces extremely rapid, robust analyses of the FTIR reflectance

data, even for very thin films in the presence of noise, and accounts for baseline shifts and curvature due to interference fringes.

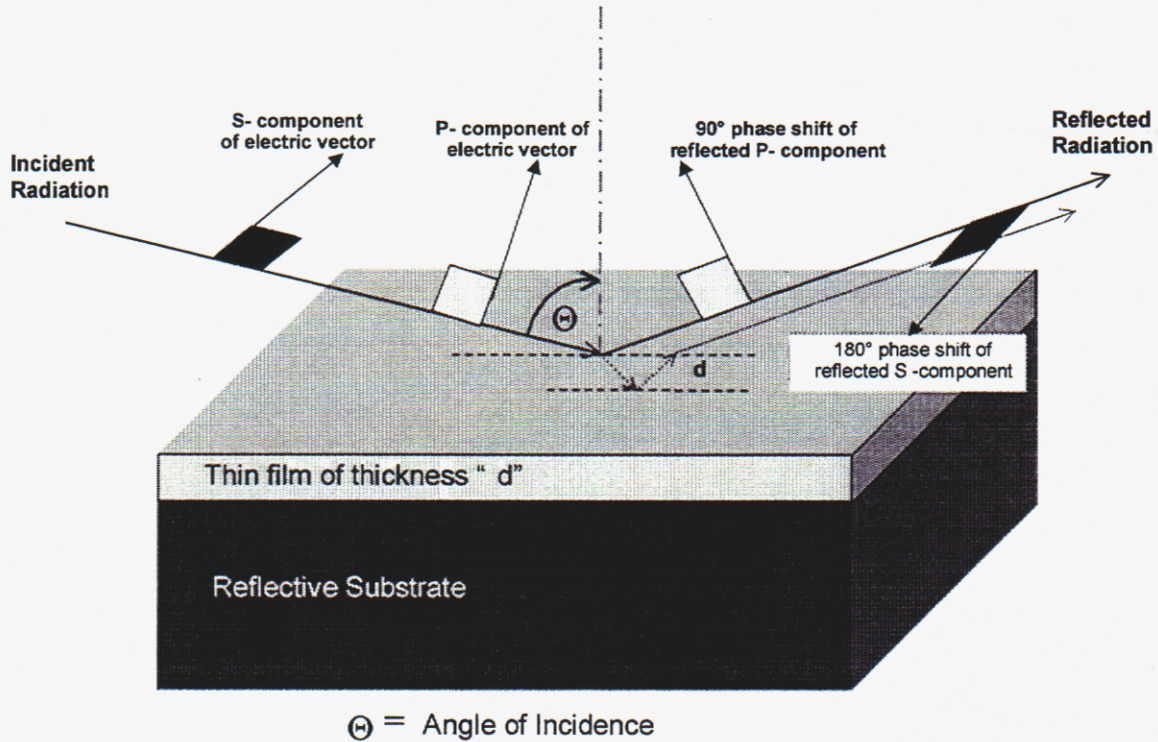


FIGURE 3. Experimental arrangement and definition of important quantities in reflection-absorption spectroscopy.

Fitting coefficients for the linear spectral function (which are proportional to the integrated intensity) are plotted against the average calculated film thickness, and these results are shown in Figures 5 and 6 for longitudinal and transverse reflectance measurements at  $75^\circ$  and  $60^\circ$  angle-of-incidence. Results for the longitudinal,  $60^\circ$  angle-of-incidence follow a linear relationship with film thickness except for the roughest surface finish ( $80$  grit,  $R_a = 6 \mu\text{m}$ ). The instrument response functions for transverse measurements at  $60^\circ$  angle-of-incidence are also reasonably linear, with the same average slope as seen in Figure 5.

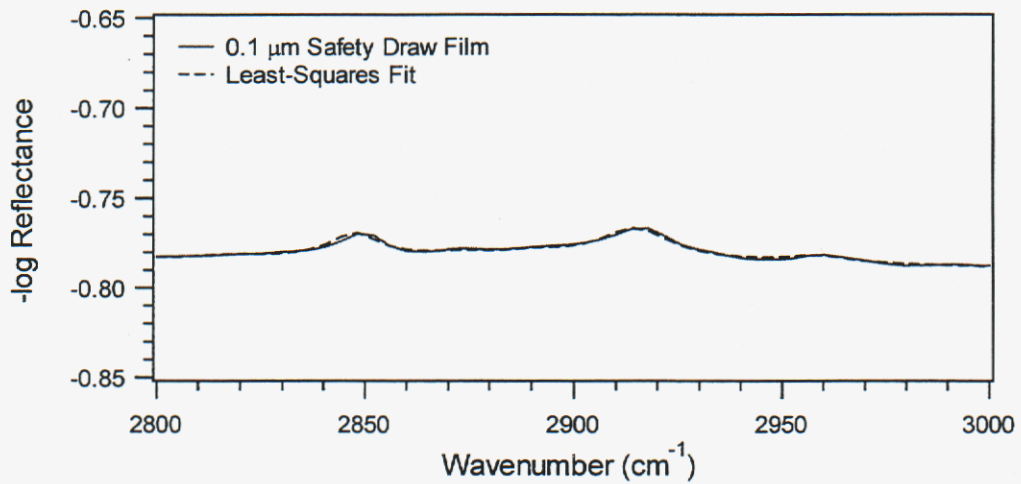
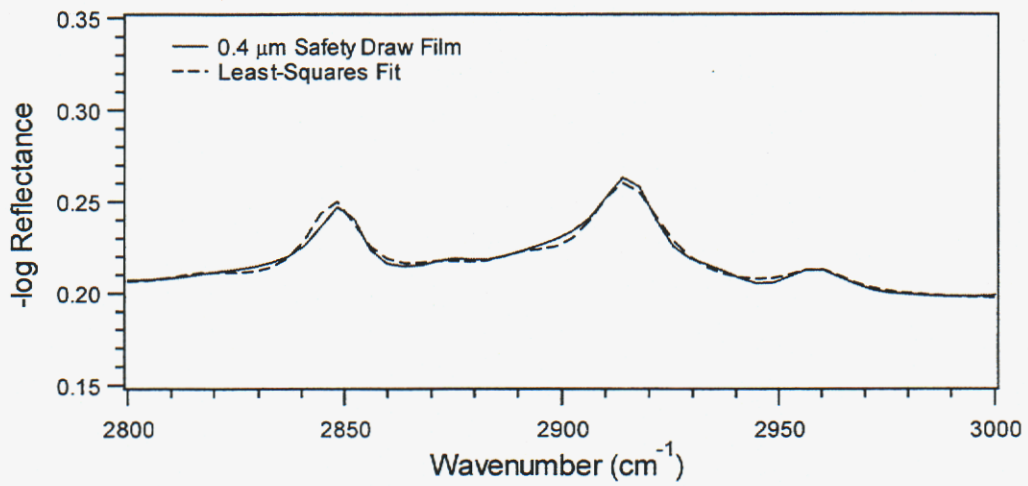
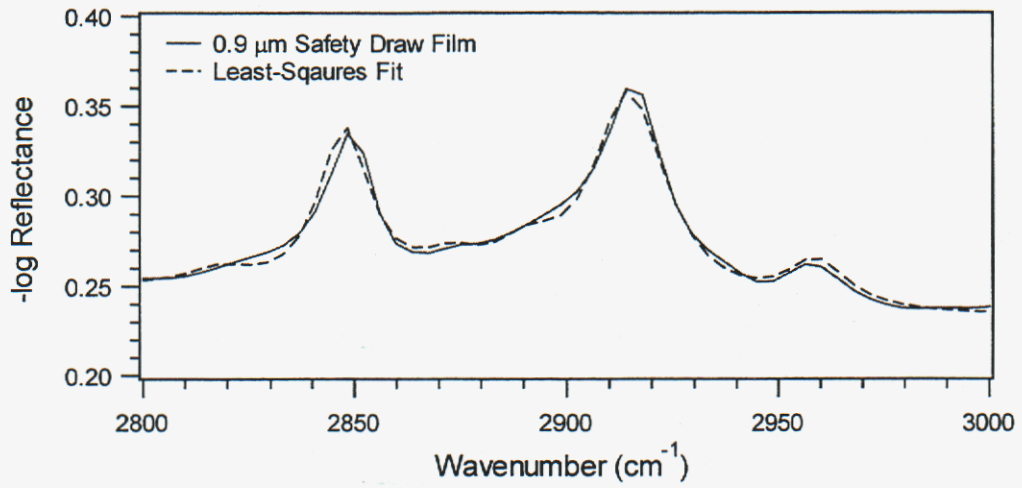


FIGURE 4. Linear least-squares fit of experimental reflectance data for drwaing-agent contaminant on 600 grit polished aluminum surfaces. Average film thickness: (Top) 0.9  $\mu\text{m}$ , (Middle) 0.4  $\mu\text{m}$ , (Bottom) 0.1  $\mu\text{m}$ .

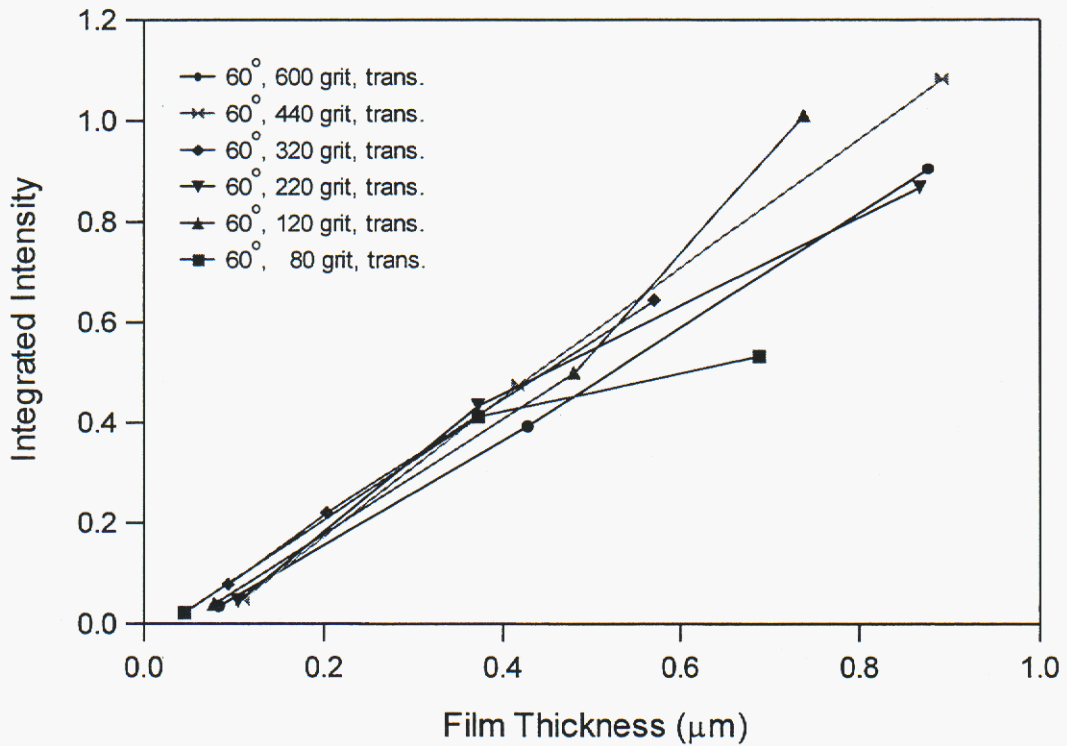
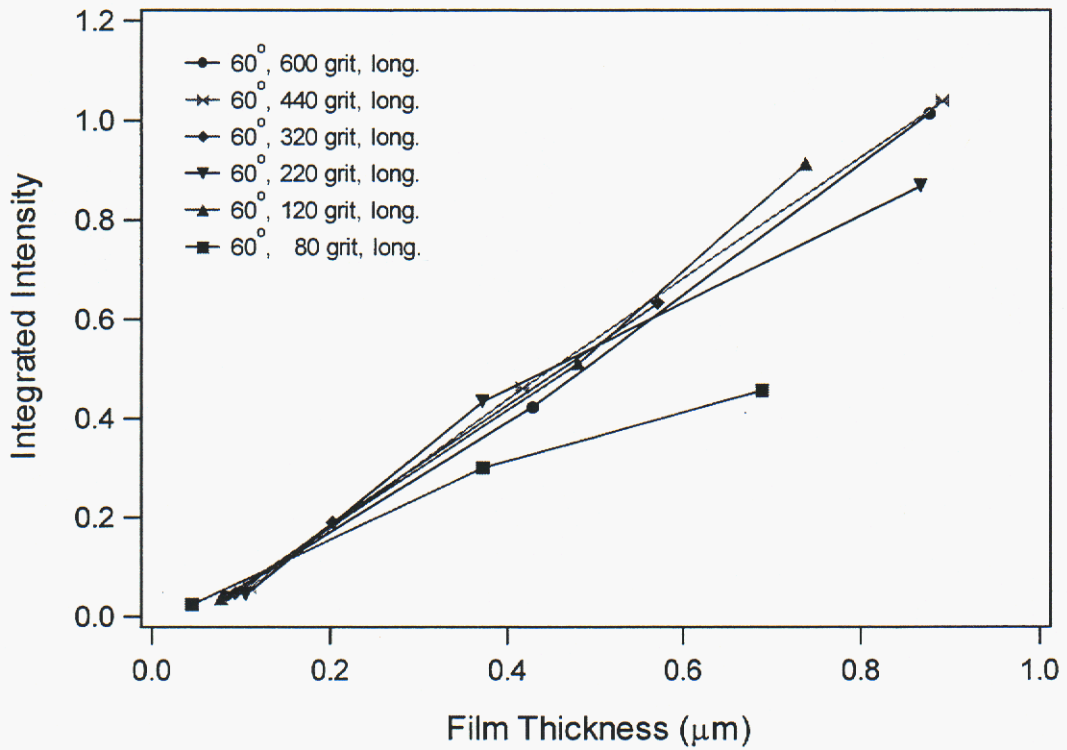


FIGURE 5. Integrated reflection-absorption intensity at 60° angle-of-incidence for C-H stretching bands of drawing-agent films deposited on aluminum test coupons with varying degrees of surface roughness (longitudinal, top; transverse, bottom).

In contrast, analysis of the FTIR reflectance data at 75° angle-of-incidence for both longitudinal and transverse sample orientations shows a marked departure from linearity at the highest values of film thickness (Figure 6). Initial slopes in integrated reflection-absorption intensity in these figures are slightly greater than the 60° angle of incidence data (Figure 5). This behavior is expected due to the increase in reflection-absorption sensitivity with increasing angle of incidence. Here, too, the average initial slope (and hence instrument sensitivity) is the same for both transverse and longitudinal orientations.

The pronounced non-linearity in slope for the thickest films at 75° angle-of-incidence was unexpected. An increasingly non-linear response may be observed for thicker absorbing films, and this effect will become more pronounced as the angle of incidence is also increased. Such an interpretation of the current results is not substantiated by calculated spectra for the present measurement conditions, however, due to the small change from 60 to 75° in angle of incidence. Furthermore, such a non-linear effect would be most pronounced for measurements on the smoothest substrate (Figure 6, filled circles) where the effective local orientation of the surface is most constant with respect to the illumination beam. These are by far the most linear sample series for the 75° data.

We attribute the pronounced non-linearity of the 75° data for the thickest drawing-agent films to the morphological characteristics of the material as deposited on the aluminum test panel surface. As described above, the drawing-agent material is highly viscous and forms a visibly heterogeneous white film at 1- $\mu\text{m}$  thickness. Variations in the deposition process produce relatively thick local areas of drawing-agent film and result in accretion of solid residue along the polishing grooves and ridges of the aluminum substrate. Under these circumstances, illumination of the surface with the FTIR beam at an angle of 75° may result in shadowing by contaminant material on ridge structures for all except the smoothest (600 grit polish) surface.

The 12-mm diameter focal area of the infrared beam is elongated by a factor of four for this angle of incidence. In contrast, reflectance measurements at 60° result in only a factor of 2 elongation, and minimize the shadowing effect of thick films except for ridges on the roughest (80 grit polish) surfaces.

This interpretation is substantiated by reflectance data for the second test set (lubricant material) as shown in Figure 7. FTIR reflectance measurements have been made at 75° angle-of-incidence for a test series similar to that of the drawing-agent set. A preliminary analysis of the C-H stretching frequencies shows a strikingly more linear dependence of instrument response with film thickness (with the exception of a single point for one of the panels with a 220 grit surface finish). We believe that this is due to the more fluid characteristic of the lubricant material, which allows the deposited film to conform much more closely to the surface topography of the test coupons. This behavior may also account for the stronger dependence of the integrated intensity slope with surface roughness, when compared to the nearly constant results for the drawing-agent contaminant examined above.

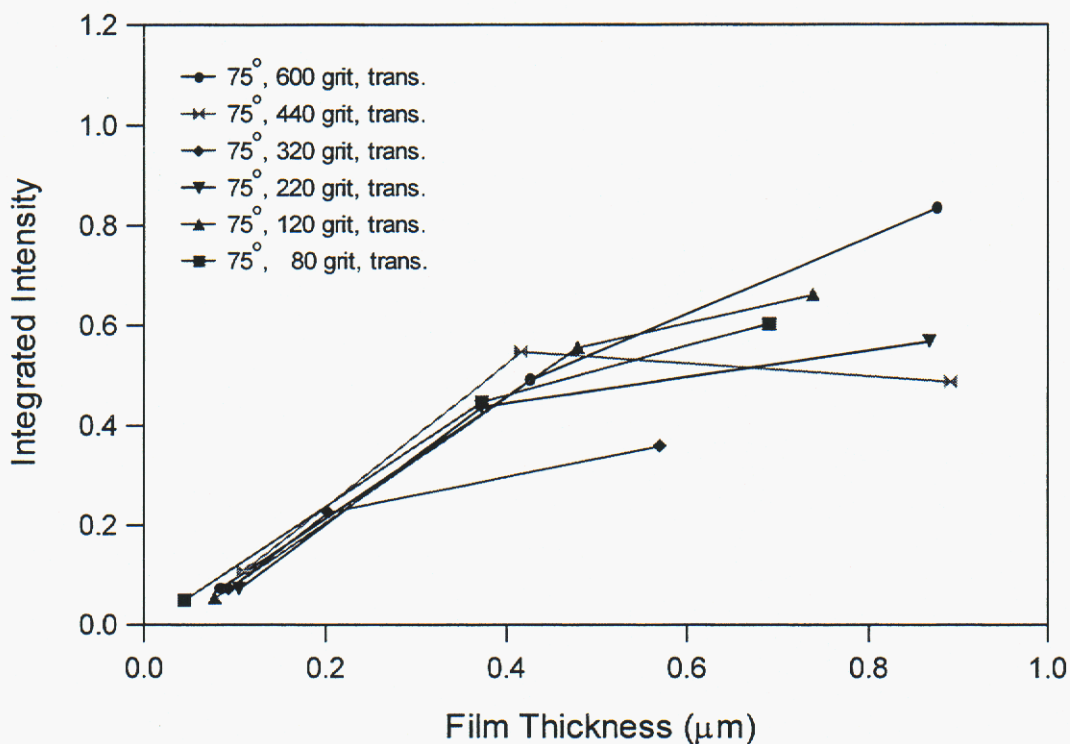
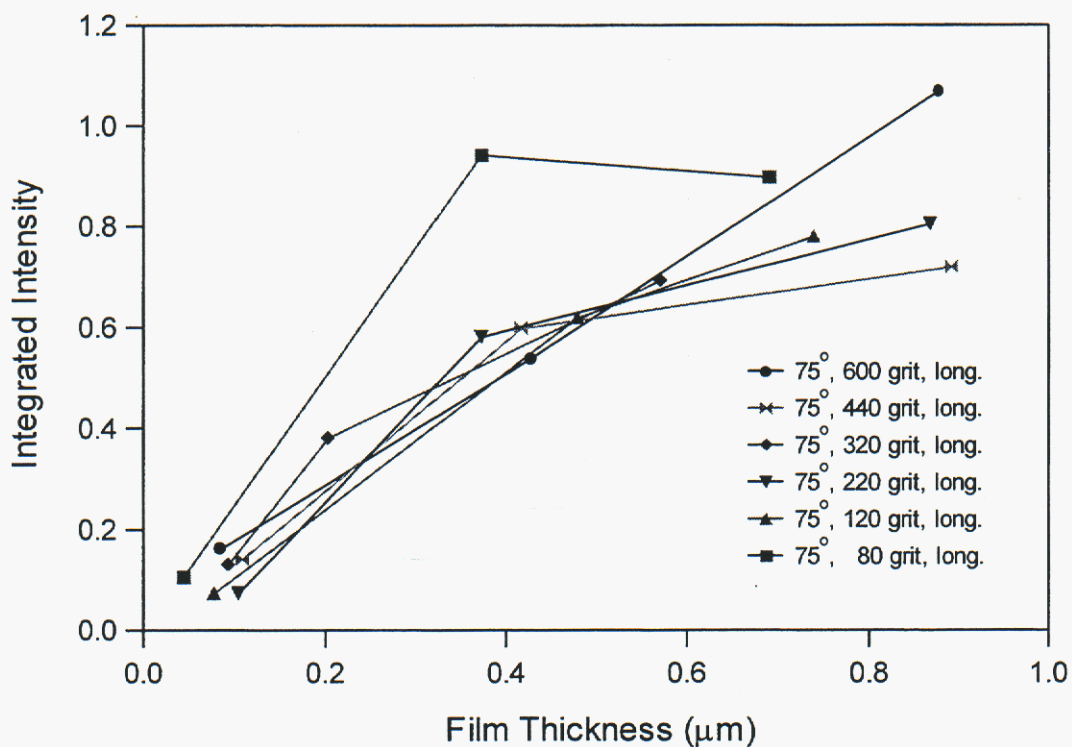


FIGURE 6. Integrated reflection-absorption intensity at 75° angle-of-incidence for C-H stretching bands of drawing-agent films deposited on aluminum test coupons

with varying degrees of surface roughness (longitudinal, top; transverse, bottom).

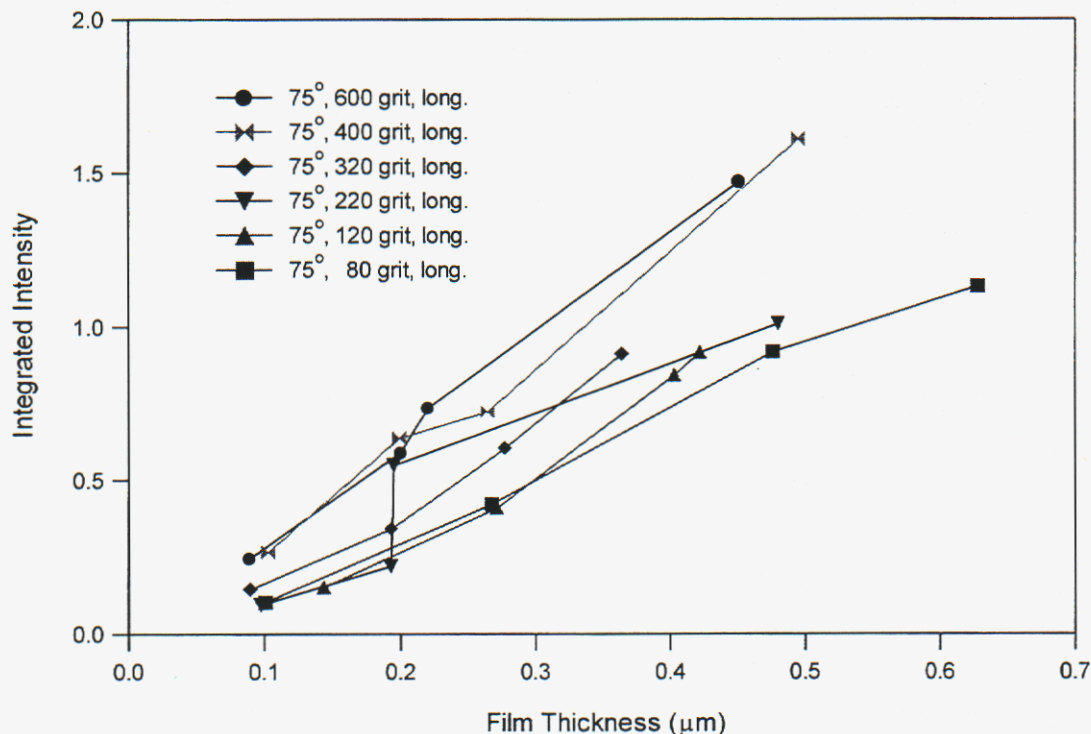


FIGURE 7. Reflection-absorption intensities of C-H stretching bands for lubricant films deposited on aluminum test coupons with varying degrees of surface roughness.

Even though excellent sensitivity was demonstrated for common hydrocarbon contaminants using grazing-angle infrared reflectance spectroscopy, concerns remain due to potential interference from other molecular species that may be present in the measurement environment. Chief among these is water, resulting either from cleaning operations or the local environment. Water is a very strong infrared absorber, and its presence on the surface to be measured may cause distortion or obscuration of the characteristic contaminant reflection spectrum.

We performed an evaluation of this interference using lubricant-contaminated test panels with an average hydrocarbon thickness of  $0.7 \mu\text{m}$  on aluminum. A water film was created on the surface

of the test coupon using an air brush, and reflection-absorption measurements were acquired at 75° angle of incidence for several conditions. The thickness of the water film was difficult to determine due to continuous evaporation during the reflectance measurement. We estimated the thickness by measuring coupon weight gain immediately prior to and following the infrared measurement. Film thickness was calculated based on the average weight gain.

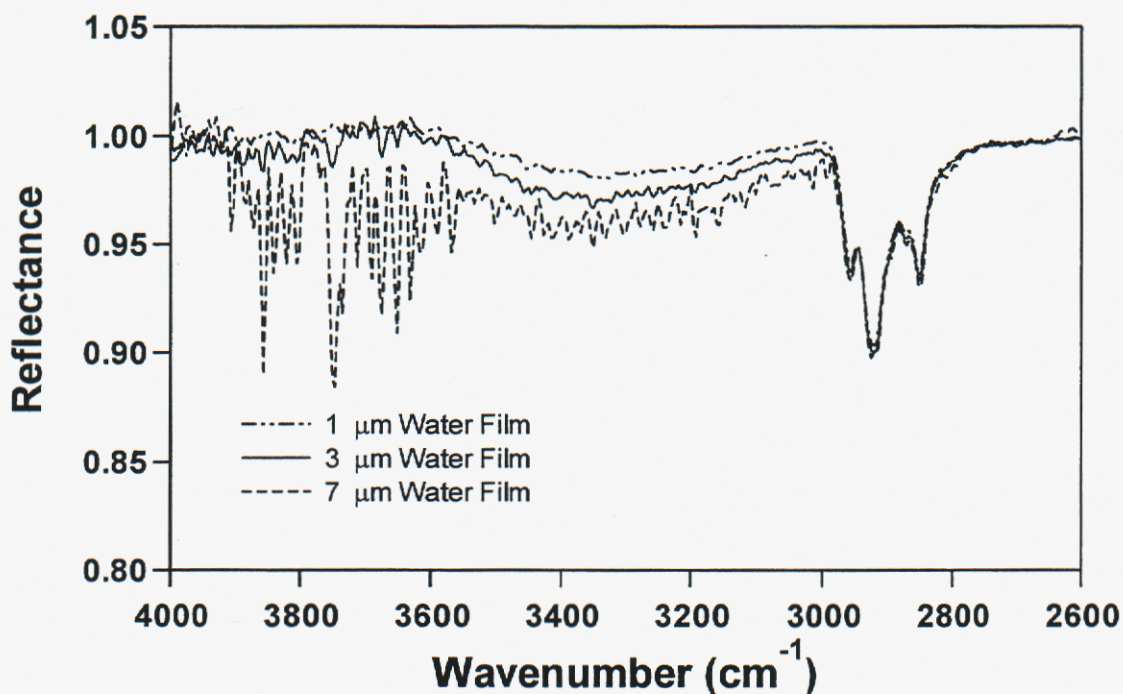


FIGURE 8. Potential interference effects of water on C-H stretching bands of hydrocarbon lubricant film (0.7 μm) on aluminum. Three thicknesses of water film are examined (1 μm, top; 3 μm, middle; and 7 μm, bottom).

Reflection-absorption spectra are presented in Figure 8 for three water films on the lubricant-contaminated test panel. These water films range in thickness from 1 μm (not visible to the eye) to 7 μm (clearly visible to the eye). Substantial interference is present in the 1700 cm<sup>-1</sup> spectral range (not shown) due to the strong H-O-H bending mode. This strong absorption obscures carbonyl absorption features that may be present in some, but not all, hydrocarbon contaminant species. The C-H stretching bands near 2900 cm<sup>-1</sup>, however, are not obscured by the broad H-OH stretching bands centered near 3400 cm<sup>-1</sup>. This is particularly important for the effective and

accurate use of the tunable infrared-laser imaging instrument, since images are acquired for only a small number frequencies near  $3000\text{ cm}^{-1}$  in contrast to the broad-band spectral data collected by the FTIR instrument.

### **Tunable Infrared-Laser Imaging**

Raw images of test panel surfaces are acquired at two frequencies ( $2915$  and  $3000\text{ cm}^{-1}$ ) that correspond to highly absorbing and non-absorbing portions of the hydrocarbon infrared spectrum (see above, Figures 4 and 8). We use an acquisition time of  $0.5\text{ ms}$  per frame, and average a minimum of 20 frames for each frequency in order to reduce noise (shot noise and laser speckle noise). Although the InSb FPA camera is square ( $256 \times 256$  pixels), the aspect ratio of the resulting images in this work are elongated by a factor of two due to the  $60^\circ$  angle of incidence and reflectance.

Images are corrected for thermal background emission and are normalized for system spectral response at the two measurement frequencies. The normalization factor is determined by the average intensity ratio of a clean surface (the uncontaminated back surface of the test panel) for the two measurement frequencies. Ratios of successive images using the PPLN-based laser system show a noise level of  $0.44\%$  for the entire  $65,536$ -pixel image under our current operating conditions. This noise level corresponds to a hydrocarbon film thickness of approximately  $10 - 20\text{ nm}$  for the species examined in this report, and is the primary factor in determining the present instrumental detection limit.

Gray-scale images at these two frequencies for the hydrocarbon drawing-agent (thickness of  $0.9\text{ }\mu\text{m}$  on aluminum) are shown in Figure 9. Structure in the images is primarily in the form of vertical lines that represent ridges in the aluminum substrate formed during surface polishing operations. The presence of an absorbing hydrocarbon in the  $2915\text{ cm}^{-1}$  image is manifested by a darker vertical band near the center of the image. However, it is difficult to differentiate the absorbing organic film from the high contrast presented by the surface polishing marks in images at a single wavelength.

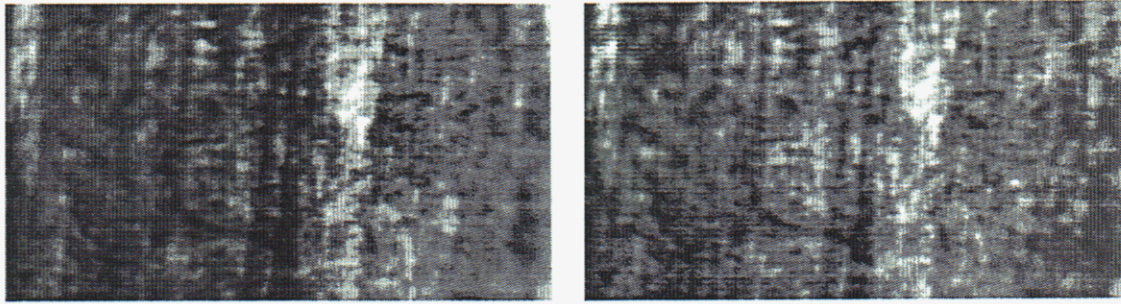


FIGURE 9. Gray-scale images on-resonance ( $2915\text{ cm}^{-1}$ , left) and off-resonance ( $3000\text{ cm}^{-1}$ , right) for an aluminum test panel contaminated with hydrocarbon drawing agent of  $0.9\text{-}\mu\text{m}$  thickness.

The ratio of these corrected and normalized images forms a relative reflectance image, as shown in Figure 10, assuming that the reflectance of the substrate remains constant at these two frequencies. Unprocessed image ratios such as this show a periodic grid pattern due to coherent interference effects that tend to obscure the hydrocarbon image, and we have investigated several image enhancement procedures to reduce noise while maintaining spatial resolution and contrast in the reflectance ratio images. Weighted Gaussian smoothing in a  $7 \times 7$  pixel neighborhood and Fourier filtering have both been successful in suppressing this noise without significant degradation in spatial resolution, as shown in Figure 10. The image ratios presented in this report have all been Gaussian smoothed. Reflectance intensity profiles along the horizontal black line in each image ratio are also shown in Figure 10 to demonstrate the magnitude of laser coherence noise and the effects of the smoothing procedure.

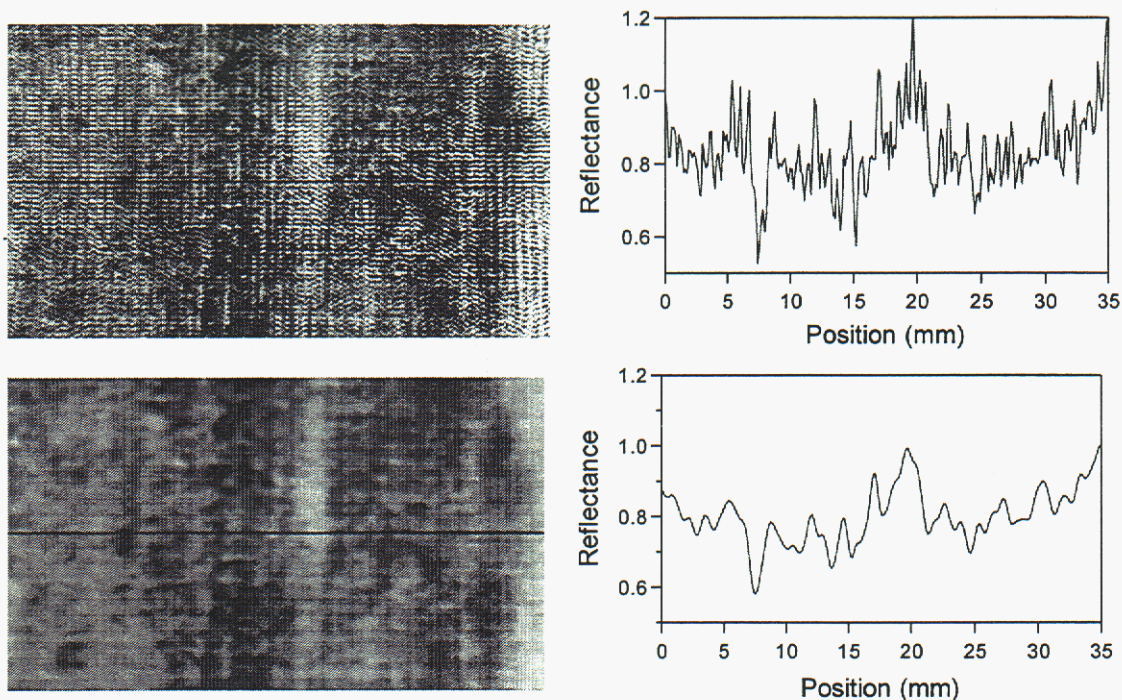
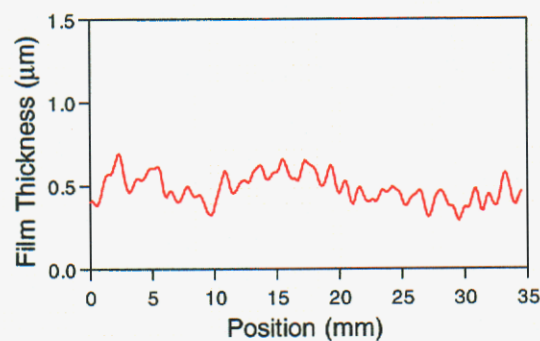
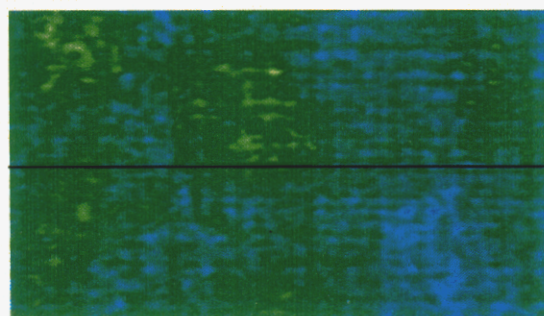
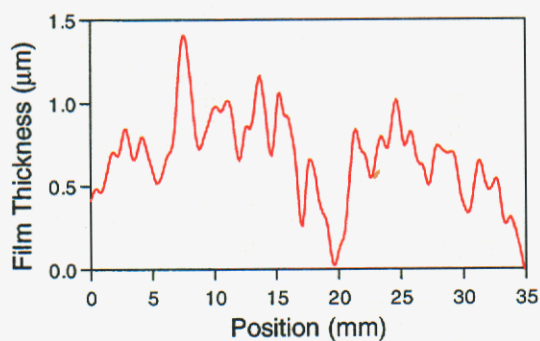
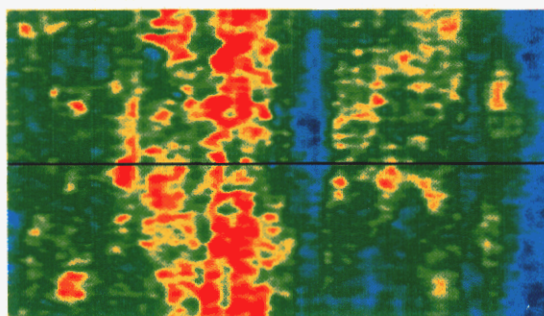


FIGURE 10. Reflectance images and line-intensity profiles for an aluminum test panel contaminated with drawing-agent hydrocarbon of 0.9- $\mu\text{m}$  thickness. Laser coherence noise (top, left) and results of Gaussian smoothing (bottom, left) are illustrated with corresponding intensity profiles (top and bottom right, respectively) for the horizontal lines superimposed on the images.

Examples of reflectance ratio images for several test surfaces are shown below in Figures 11 and 13 in false color. A calibrated color-table (“Rainbow”) for these false-color images is shown in Figure 12. Images for a series of 600-grit polished aluminum substrates contaminated with drawing agent are presented in Figure 11. These are the same specimens whose FTIR spectra are shown in Figure 4. Average film thicknesses for the three samples are 0.9  $\mu\text{m}$  (top, left), 0.4  $\mu\text{m}$  (middle, left), and 0.1  $\mu\text{m}$  (bottom, left).

The images are presented in false color format with identical dynamic range to help visualize the location of contaminants. Hydrocarbon material was manually deposited along the orientation of the surface polishing grooves which is oriented vertically in these images. Heavy deposits of the

hydrocarbon residue are easily visible in the top reflectance image (red and yellow indicating the lowest reflectance, hence the thickest deposit, locations), with a particularly thick vertical band near the center. Very few areas in this image possess high reflectance values (dark blue) characteristic of low contamination. A horizontal line across the center of the image indicates the location of the thickness profile for this sample (Fig. 11, top, right). Reflectance values have been converted to thickness of the drawing-agent hydrocarbon contaminant using the FTIR data analysis discussed above. The data shown here indicate the thickness averaging about  $0.7 \mu\text{m}$  along the profile line, with heavier deposits up to  $2 \mu\text{m}$ .



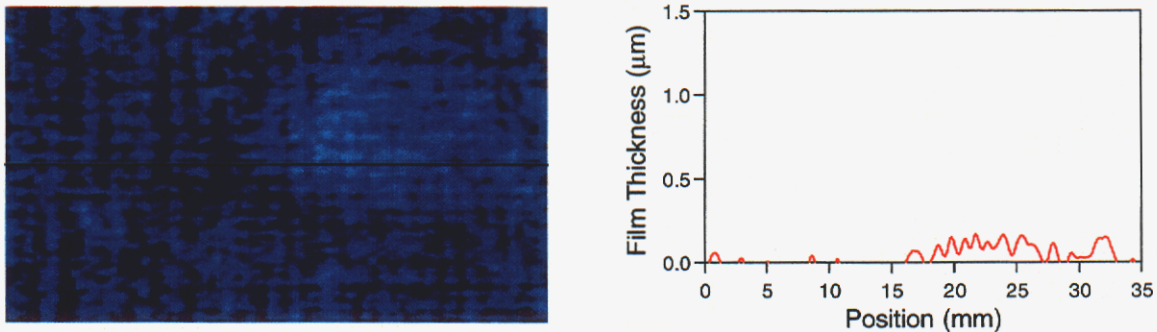


FIGURE 11. False-color reflectance images and thickness profiles for three aluminum test panels contaminated with Safety Draw hydrocarbon drawing agent (thicknesses are: 0.9  $\mu\text{m}$ , top-left; 0.4  $\mu\text{m}$ , middle-left; 0.1  $\mu\text{m}$ , bottom-left). Corresponding line thickness profiles are shown to the right of each false-color image.

False color images of the test surfaces contaminated with lower amounts of hydrocarbon (Fig. 11, middle and bottom) show much less spatial variation in the distribution of hydrocarbon residue. Hydrocarbon residues are thinner and appear as predominantly green and light blue in the false-color images, respectively, while the line profiles show quantitatively the thickness of lubricant in these images. The average values of the three profiles presented here are consistent with the weight change and FTIR calibration data.

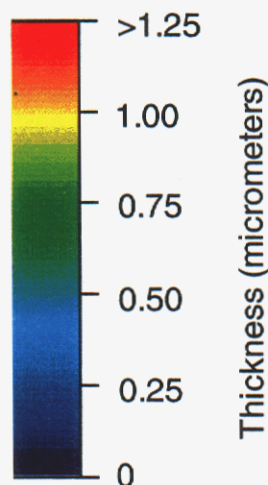
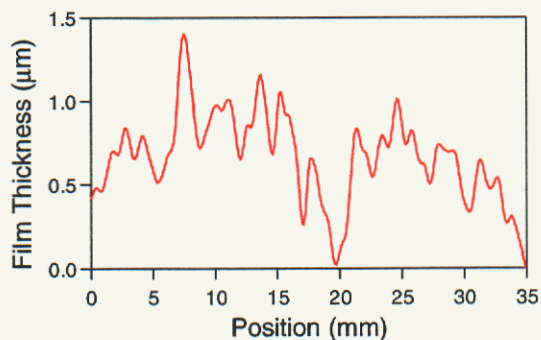
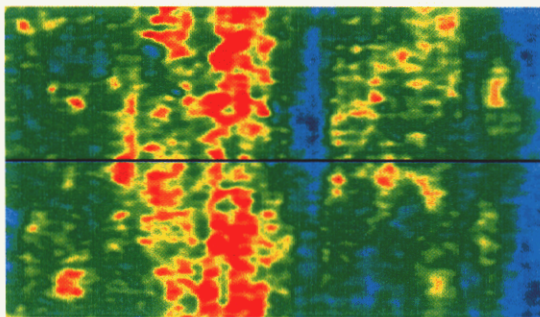


FIGURE 12. Color table for false-color images presented in Figures 11 and 13. Calibration of film thickness was calibrated by weight-gain measurements during sample preparation, and comparison with FTIR reflectance data (see above).

The potential value of the infrared-laser imaging method for cleaning verification is clearly demonstrated for these test panels. For these samples distribution of the residual hydrocarbon contaminant is quite variable. In the case of the heaviest contaminated sample, localized cleaning to effect substantial removal can be profitably applied to the most heavily contaminated areas.

We also acquired reflectance ratio images for test surfaces with rougher finishes for average hydrocarbon thicknesses of 0.9  $\mu\text{m}$ . False-color images and corresponding thickness profiles for these two samples are compared to the 0.9- $\mu\text{m}$  thick hydrocarbon residue deposited on the smoothest, 600-grit polished surface in Figure 13. Average thickness values from the three profiles are in reasonable agreement for all three test panels, demonstrating that large changes in surface roughness (0.5, 2.1, and 6.1  $\mu\text{m}$ ) do not substantially affect the measured thickness of hydrocarbon residue.

We observe a qualitative change in the false-color images in Figure 13. Increasingly rough test surfaces (middle and bottom) exhibit a more grainy image quality due to the large diversity of surface orientations relative to the infrared laser illumination beam. Distribution of the hydrocarbon residue on the 220-grit surface, however, is much more even (Fig. 13, middle, left) than for the smoothest surface (Fig. 13, top, left). The drawing-agent material shows a strong thickness gradient toward the right-hand side of the image for the roughest, 80-grit, surface (Fig. 13, bottom, left) that is clearly visible despite the grainy image appearance.



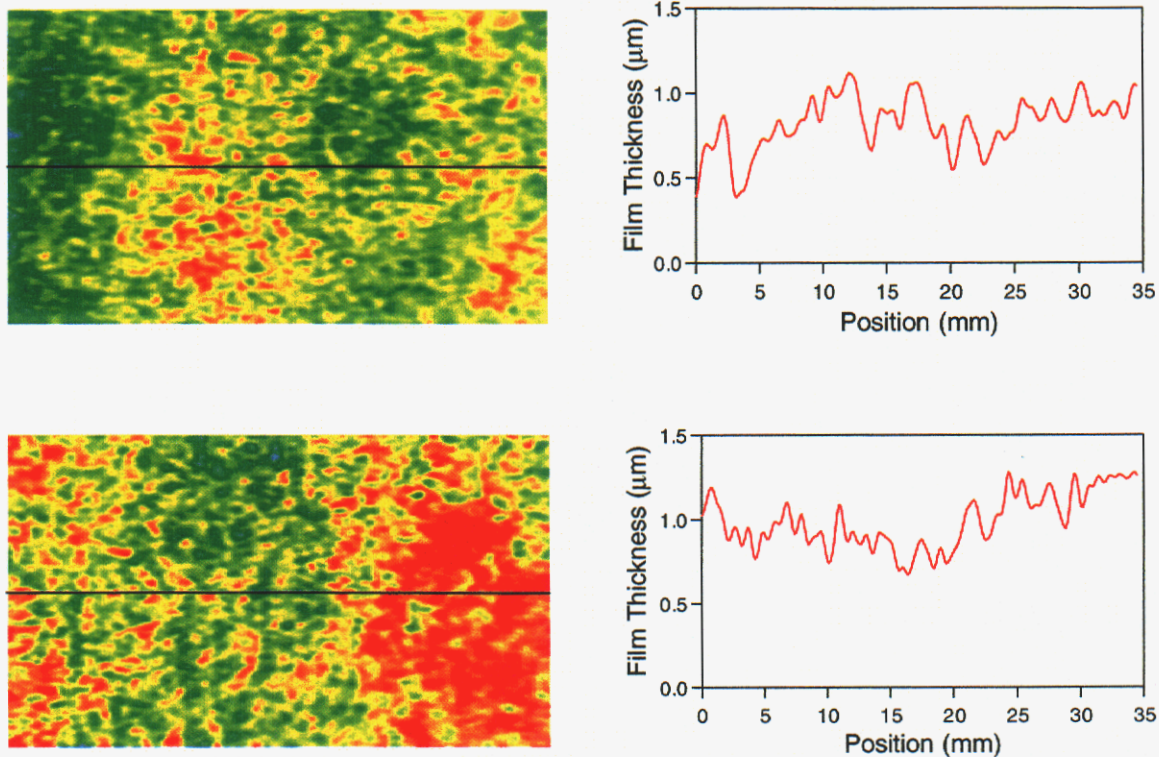


FIGURE 13. False-color reflectance images and thickness profiles for three aluminum test panels with drawing-agent hydrocarbon contaminant (surface polishes are: 600-grit, top-left; 220-grit, middle-left; 80-grit, bottom-left). Corresponding line thickness profiles are shown to the right of each false-color image.

#### IV. Conclusions

The work presented in this report has shown tunable infrared-laser imaging to be an extremely attractive method for on-line for the detection of hydrocarbon contaminants and determination of their spatial distribution for efficient cleaning operations. Calibrated test panels of hydrocarbon contaminants on metallic substrates were prepared and characterized with FTIR grazing-angle reflectance spectroscopy. Measurements were made over a range of film thicknesses and surface roughness, and the derived instrument sensitivity was quite robust with respect to the degree of surface roughness and the orientation of the reflectance unit to the direction of polishing grooves.

Tunable infrared-laser images were acquired at absorbing and non-absorbing frequencies for hydrocarbon contaminants on aluminum test panels, and showed good agreement in measured film thickness with spatially averaged FTIR spectroscopic results. The laser images clearly reveal the heterogeneous distribution of the contaminant species on the component surfaces for a variety of film thicknesses and degree of surface roughness.

Current detection limits of the laser-imaging method are determined primarily by the effects of laser-coherence noise when image ratios are formed for absorbing and non-absorbing wavelengths. For typical hydrocarbon species, the detection limit appears to be on the order of 10 – 20 nm for film thickness. Improvements in the system despeckling and projection optics may substantially decrease this noise level with an attendant increase in sensitivity.

The configuration of a future prototype imaging system instrument will be strongly determined by system formats that employ either a pulsed or continuous-wave laser, and staring focal-plane array (FPA) cameras or raster-scanned imagers. The design of an imaging system will include a consideration of the ultimate instrument cost. At the present time, it appears that a continuous-wave system with a scanned imager offers the lowest cost. However, the performance of some newly developed inexpensive infrared microbolometer arrays will also be evaluated as a possible component of a low-cost pulsed imager.

## V. References

1. D. Allara, *The study of thin polymer films on metal surfaces using reflection-absorption spectroscopy*, in *Characterization of Metal and Polymer Surfaces*, Vol. 2, ed. Lee, (Academic Press, New York, 1977).
2. R.W. Bradshaw, D. Ottesen, L.R. Thorne, A.L. Newman, and L.N. Tallerico, Sandia Report, Sandia National Laboratories, SAND87-8241 (December 1987).
3. J. Greenler, *Chem. Phys.*, 310 (1966).
4. W. G. Golden, *Fourier transform infrared reflection-absorption spectroscopy*, in *Fourier Transform Infrared Spectroscopy*, Vol. 4, (Academic Press, New York, 1985).
5. T. A. Hoffard, C. A. Kodres, D. R. Polly, *Grazing-angle Fourier transform infrared spectroscopy for online surface cleanliness verification*, NFESC Technical Memorandum, NFESC-TM-2335-SHR (2000).
6. C. A. Kodres, D. R. Polly, and T. A. Hoffard, *Surface quality impact of replacing vapor degreasers with aqueous immersion systems*, NFESC Technical Report, NFESC-TR-2067-ENV (1997).
7. C. A. Kodres, D. R. Polly, and T. A. Hoffard, *Surface quality impact of cleaning systems*, (Metal Finishing, 1997), p.48.
8. Ottesen, D., *J. Electrochem. Soc.*, 1985, 2250.
9. Ottesen, D., Thorne, L. R., and Bradshaw, R. W., Sandia Report SAND86-8789 (June, 1986).
10. P.E. Powers, T.J. Kulp, and S.E. Bisson, *Continuous tuning of a cw PPLN OPO using a fan-out grating design*, accepted for publication, (Optics Letters, November, 1997).

## VI. DISTRIBUTION

- 5        3M Corp.  
          3M Center  
          Attn: Pete Ludowise  
          Bldg. 270-2N-15  
          Maplewood, MN 55144
- 1        American Iron and Steel Institute  
          Attn: Joseph Vehec  
          247 Fort Pitt Blvd.  
          Second Floor  
          Pittsburgh, PA 15222
- 1        Bethlehem Steel Corp.  
          Attn: Tim Miller  
          Homer Research Labs  
          Bethlehem, PA 18016
- 1        Boeing Commercial Airplanes  
          Attn: Paul Shelley  
          PO Box 3707 M/C 9U-EA  
          Seattle, WA 98124-2207
- 1        Boeing Company  
          Attn: Stephen Gaydos  
          PO Box 516  
          MC S034-1126  
          St. Louis, MO 63166-0516
- 1        Corning, Inc.  
          Attn: Uta Goehrs  
          Mail Stop SP-TD-01-2  
          Corning, NY 14831
- 1        ESTCP Program Office  
          Attn: Jeffrey Marqusee  
          901 N. Stuart Street  
          Suite 303  
          Arlington, VA 22203

- 5 Intel Corporation  
CH5-232  
Attn: Scott Robinson  
5000 W. Chandler Blvd.  
Chandler, AZ 85226-3699
- 1 Materials & Manufacturing Technology Directorate  
Wright Laboratory (AFRL/MLQ)  
Attn: Tom Naguy  
2179 Twelfth St., Rm 122  
Wright Patterson AFB, OH 45433-7718
- 1 Naval Aviation Depot, North Island  
Attn: Tim Woods  
PO Box 357058  
San Diego, CA 92135-7058
- 1 Naval Aviation Depot, North Island  
Attn: Doug Perl  
PO Box 357058  
San Diego, CA 92135-7058
- 5 Naval Facilities Engineering Service Center  
Code ESC63  
Attn: Theresa Hoffard  
1100 23<sup>rd</sup> Avenue  
Port Hueneme, CA 93043-4370
- 1 OO-ALC/TIELM  
Attn: Richard Buchi  
7278 4<sup>th</sup> Street  
Bldg 100, Bay D  
Hill Air Force Base, UT 84056-5205
- 1 OO-ALC/TIELM  
Attn: Wayne Patterson  
7278 4<sup>th</sup> Street  
Bldg 100, Bay D  
Hill Air Force Base, UT 84056-5205
- 1 SERDP Program Office  
Attn: Charles Pellerin  
901 N. Stuart Street  
Suite 303  
Arlington, VA 22203

1 SERDP Program Office  
Attn: Bradley Smith  
901 N. Stuart Street  
Suite 303  
Arlington, VA 22203

1 Surface Optics Corp.  
Attn: Martin Szczesniak  
11555 Rancho Bernardo Road  
San Diego, CA 92127-1441

1 Surface Optics Corp.  
Attn: Mark Dombrowski  
11555 Rancho Bernardo Road  
San Diego, CA 92127-1441

1 The Timken Company  
Mail Code GNW-07  
Attn: Bob Kolarik  
PO Box 6932  
Canton, OH 44706-0932

1 Weirton Steel Corp.  
Attn: Ted Polas  
400 Three Springs Road  
Weirton, WV 26062-4989

1 MS 9001 M. E. John, 8000  
Attn: R. C. Wayne, 2800, MS 9005  
J. Vitko, 8100, MS 9004  
W J. McLean, 8300, MS 9054  
D. R. Henson, 8400, MS 9007  
P. N. Smith, 8500, MS 9002  
K. E. Washington, 8900, MS 9003  
D. L. Crawford, 9900, MS 9003

1 MS 9051 L. A. Rahn, 8351  
1 MS 9051 K. M. Armstrong, 8356  
1 MS 9051 S. E. Bisson, 8356  
1 MS 9051 D. A. V. Kliner, 8356  
1 MS 9051 T. J. Kulp, 8356  
1 MS 9051 T. A. Reichardt, 8356  
1 MS 9051 P. M. Walsh, 8356  
1 MS 9052 S. W. Allendorf, 8361

1	MS 9052	B. T. Chorpening, 8361
1	MS 9052	D. R. Hardesty, 8361
1	MS 9052	C. R. Shaddix, 8361
1	MS 9054	B. J. McLean, 8300
1	MS 9056	R. J. Gallagher, 8356
1	MS 9105	J. A. Lamph, 8119
1	MS 9105	M. C. Stoddard, 8119
1	MS 9161	K. F. McCarty, 8721
1	MS 9402	W. R. Even, 8722
1	MS 9402	K. L. Wilson, 8724
1	MS 9403	H. A. Johnsen, 8723
1	MS 9403	B. E. Mills, 8723
20	MS 9403	D. K. Ottesen, 8723
1	MS 9403	E. E. Tarver, 8723
2	MS 9403	J. C. F. Wang, 8723
1	MS 9131	K. D. Overby, 8528
1	MS 9405	R. H. Stulen, 8700
		Attn: J. M. Hruby, 8702, MS 9401
		W. Bauer, 8704, MS 9161
		R Q. Hwang, 8721, MS 9161
		W. A. Kawahara, 8725, MS 9042
		E. P. Chen, 8726, MS 9161
		J. L. Handrock, 8727, MS 9042
		M. F. Horstemeyer, 8728, MS 9042
		C. C. Henderson, 8729, MS 9401
		J. E. M. Goldsmith, 8730, MS 9055
		W. C. Replogle, 8731, MS 9409
		G. D. Kubiak, 8732, MS 9409
3	MS 9018	Central Technical Files, 8945-1
1	MS 0899	Technical Library, 9616
1	MS 9021	Classification Office, 8511/Technical Library, MS 0899, 9616
1	MS 9021	Classification Office, 8511 for DOE/OSTI